

Cellulose

Comparative Study of Historical Woods from XIX Century by Thermogravimetry coupled with FTIR Spectroscopy --Manuscript Draft--

Manuscript Number:	CELS-D-19-00636
Full Title:	Comparative Study of Historical Woods from XIX Century by Thermogravimetry coupled with FTIR Spectroscopy
Article Type:	Original Research
Keywords:	Historical Woods; Thermogravimetry; FTIR spectroscopy; Wood pyrolysis; Non isothermal thermogravimetric analysis.
Abstract:	<p>Thermal and structural properties of historical woods from apparatuses of the Historical Collection of the Physics Instruments of the University of Palermo have been investigated by FTIR spectroscopy coupled with thermogravimetric (TG) analysis. Specifically, the wooden portions of apparatuses from XIX century have been studied. The thermal behavior of the wooden materials has been successfully interpreted on the basis of specific indexes determined by the quantitative analysis of the FTIR spectra. The kinetics of the wood pyrolysis have been investigated by using a non-isothermal approach based on model-free isoconversional procedures, such as Kissinger–Akahira–Sunose (KAS) and Friedman methods. Interestingly, the activation energy of the pyrolysis process reflects both the peculiar composition (related to the specific wooden taxon) and the conservation state of the historical woods. The thermogravimetric parameters have been correlated to the lignin index of the woods by proper experimental equations, which can be considered as a novel protocol to estimate the preservation conditions of historical woods from different taxon.</p>

1 **Comparative Study of Historical Woods from XIX Century by Thermogravimetry coupled with FTIR**
2 **Spectroscopy**

3
4 Giuseppe Cavallaro^{a,b*}, Aurelio Agliolo Gallitto^a, Lorenzo Lisuzzo^a, Giuseppe Lazzara^{a,b}

5
6 *^aDipartimento di Fisica e Chimica - Emilio Segrè, Università degli Studi di Palermo, Viale delle Scienze, pad. 17,*
7 *90128 Palermo, Italy. E-mail:giuseppe.cavallaro@unipa.it*

8 *^bConsorzio Interuniversitario Nazionale per la Scienza e Tecnologia dei Materiali, INSTM, Via G. Giusti, 9, I-50121*
9 *Firenze, Italy.*

10
11
12
13
14
15
16
17
18
19
20
21
22
23
24
25
26
27
28
29
30 **KEY WORDS.** Historical Woods, Thermogravimetry, FTIR spectroscopy, Wood pyrolysis, Non isothermal
31 thermogravimetric analysis.

32 **Abstract**

33 Thermal and structural properties of historical woods from apparatuses of the Historical Collection of the Physics
34 Instruments of the University of Palermo have been investigated by FTIR spectroscopy coupled with
35 thermogravimetric (TG) analysis. Specifically, the wooden portions of apparatuses from XIX century have been
36 studied. The thermal behavior of the wooden materials has been successfully interpreted on the basis of specific
37 indexes determined by the quantitative analysis of the FTIR spectra. The kinetics of the wood pyrolysis have been
38 investigated by using a non-isothermal approach based on model-free isoconversional procedures, such as
39 Kissinger–Akahira–Sunose (KAS) and Friedman methods. Interestingly, the activation energy of the pyrolysis process
40 reflects both the peculiar composition (related to the specific wooden taxon) and the conservation state of the historical
41 woods. The thermogravimetric parameters have been correlated to the lignin index of the woods by proper
42 experimental equations, which can be considered as a novel protocol to estimate the preservation conditions of
43 historical woods from different taxon.

63

64

Introduction

65 Within the Cultural Heritage issues, the preservation of wooden artworks represents a challenging issue for
66 restorators and scientists because of the acidic deterioration of lignin and lignocellulosic polysaccharides (Bugg et al.
67 2011; Dedic et al. 2013; Rasmussen et al. 2017). Recent studies proved that the efficient protection of the wooden
68 structures can be achieved by the consolidation with resins (Cavallaro et al. 2017; Moise et al. 2019), sustainable
69 polymers (Walsh et al. 2017), organosilicon compounds (Broda et al. 2019) and alkaline nanoparticles, such as
70 calcium/magnesium hydroxides (Giorgi et al. 2005; Poggi et al. 2014) and nanotubes filled with antacid compounds
71 (Cavallaro et al. 2018). Prior to their preservation, the wooden artworks should be properly characterized in order to
72 determine the structural and compositional features of the woods. In this regards, an extensive investigation of the
73 wooden materials can be achieved by using several diagnostics techniques, such as Nuclear Magnetic Resonance
74 (NMR) spectroscopy (Bardet et al. 2002; Žlahtič Zupanc et al. 2019; Iwamoto et al. 2019), X-ray diffraction analysis
75 (XRD) (Carrillo-Varela et al. 2018), Fourier Transform Infrared (FTIR) spectroscopy (Popescu et al. 2007; Emmanuel
76 et al. 2015; Broda and Popescu 2019), Scanning Electron Microscopy (SEM) (Guo et al. 2006; Borysiak 2013; Lin et
77 al. 2018), Atomic Force Microscopy (AFM,) (Notley and Wågberg 2005; Casdorff et al. 2017) and thermal analyses
78 (Cavallaro et al. 2011a; Sebio-Puñal et al. 2012; Blanco et al. 2017; Girometta et al. 2017).

79 FTIR spectroscopy is a suitable and quick method to determine the molecular groups of the wood. Consequently,
80 the analysis of FTIR spectra can provide the effect of the weathering agents on the deterioration of the wood
81 component molecules (cellulose, hemicelluloses and lignin) (Emmanuel et al. 2015). In addition, the crystallinity
82 degree of the cellulose in the wooden materials can be estimated by specific indexes (total crystalline index and later
83 order index) obtained from the quantitative analysis of FTIR data (Carrillo et al. 2018).

84 Among the thermal analysis techniques, thermogravimetry (TG) revealed as an efficient tool for the characterization
85 of wooden samples. It was demonstrated (Janković 2014) that the analysis of TG curves endows to investigate the
86 decomposition processes of the major wooden components. Accordingly, thermogravimetry represents an indirect
87 method for the determination of the wood composition. Wooden samples from different *Eucalyptus* species exhibited
88 distinctive thermal decomposition processes for cellulose (Carrillo-Varela et al. 2018). Furthermore, the maximum
89 water content (MWC) of archaeological woods can be easily obtained by the thermogravimetric investigations
90 (Cavallaro et al. 2011a). The consolidation efficiencies of colophony (Cavallaro et al. 2017) and polyethylene glycols
91 (Cavallaro et al. 2018) towards wooden materials of historical value were estimated by studying the thermal
92 decomposition of treated woods through thermogravimetry.

93 The kinetics of the pyrolysis process of wood biomass samples can be studied by thermogravimetric measurements
94 using both isothermal (Janković 2014) and non-isothermal (Barneto et al. 2011; Mohomane et al. 2017) approaches.
95 Thermogravimetric kinetic studies evidenced the variable degradation state of archaeological and sound woods from
96 different taxa (*Pinus pinaster* and *Fagus sylvatica* L) on the basis of their activation energies to the pyrolysis process
97 (Cavallaro et al. 2011a). Kinetic analysis of thermogravimetric data allowed to discriminate softwood from hardwood
98 species according to peculiar variations of the activation energy values (Janković 2014).

99 Non-isothermal investigations are based on isoconversional procedures, which are model-free methods that provide
100 the activation energy without any assumptions on the reaction mechanism (Budrugaec et al. 2004; Rotaru 2016, 2017).
101 Based on the mathematical analysis of TG data, the isoconversional procedures are classified in integral and differential
102 methods (Vyazovkin et al. 2014; Budrugaec 2018).

103 Here, we investigated the structural and thermal characteristics of historical woods from apparatuses of the
104 Historical Collection of the Physics Instruments of the University of Palermo, which collects physics instruments of
105 mechanics, acoustic, calorimetry, electromagnetism and optics, dating from the XIX (Agliolo Gallitto et al. 2018), on
106 exhibit at the Department of Physics and Chemistry - Emilio Segrè, in the historical building of via Archirafi 36. In this
107 study, we explored the conservation state of acoustic apparatuses by studying the physico-chemical properties of their
108 wooden parts. Specifically, the samples were characterized through FTIR spectroscopy and thermogravimetry allowing
109 to obtain a complete description of the compositional, structural and thermal features of historical woods. The FTIR
110 and thermogravimetric results were correlated to the specific wood taxon as well as to the preservation conditions of
111 the historical apparatuses. According to the mathematical analysis of TG and FTIR data, this work opens a novel route
112 for the development of suitable protocols to study the conservation state of historical woods with their structural and
113 thermal characteristics.

114

Experimental

115

116

117 **Materials**

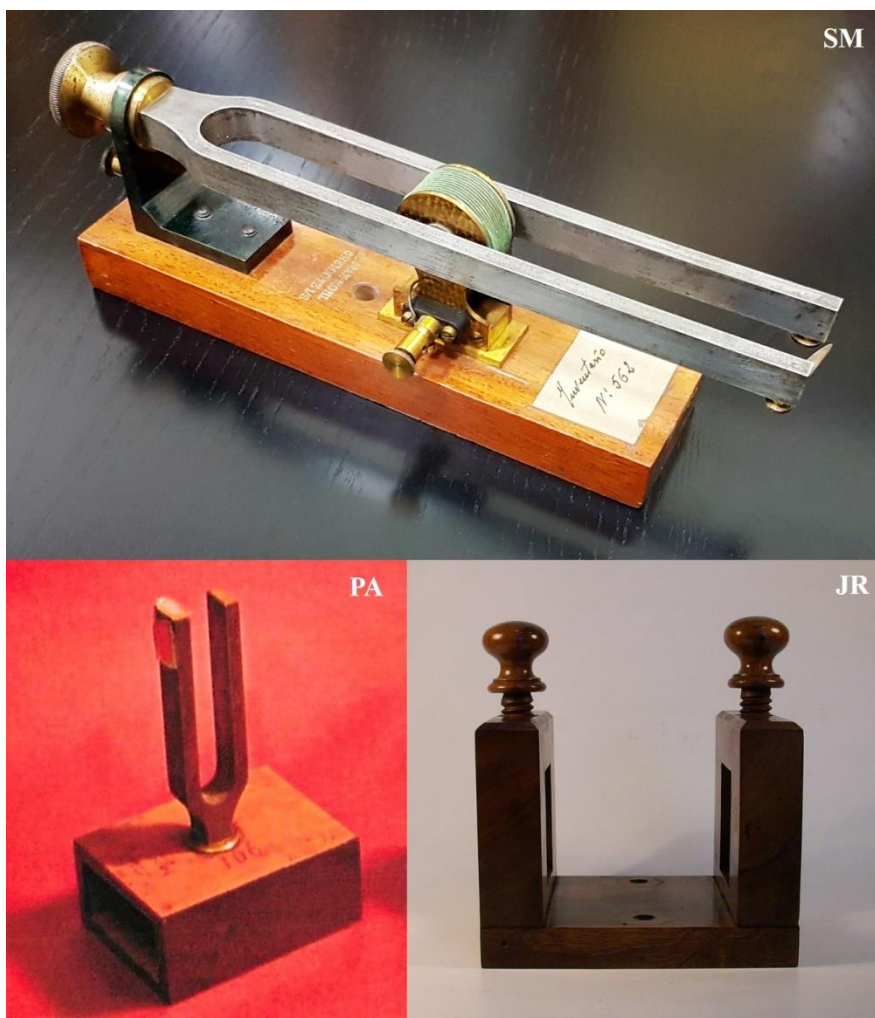
118 Three wooden samples were obtained from apparatuses of the Historical Collection of the Physics Instruments of
119 University of Palermo. In particular, one sample has been extracted from the wooden base of a chronograph tuning
120 forks with electromagnetic drive, one from the wooden resonance box of a tuning forks and one from the support for
121 tuning forks, as summarized in Table 1. As reported in Table 1, the samples differ in the age and in the wood taxon. All
122 the apparatuses (presented in Fig. 1) were manufactured in the XIX century (Agliolo Gallitto et al. 2017). In order to
123 avoid their structural deterioration, the historical wooden items are light protected and kept under controlled
124 environmental conditions. Specifically, relative humidity and temperature are set at ca. 60% and ca. 20 °C,
125 respectively.

126

127 **Table 1.** List of the historical wooden samples

Symbol	Wood taxon	Physics apparatus	Manufacturer	Year
SM	<i>Swietenia mahagoni</i>	Chronograph tuning forks with electromagnetic drive	Max Kohl, Germany	1906
PA	<i>Picea abies</i>	Tuning forks on resonance box (sound frequency of 768 Hz)	Rudolph Koenig, France	1868
JR	<i>Juglans regia</i>	Support for tuning forks	Rudolph Koenig, France	1864

128



129

130 **Fig. 1.** Photos of the physics apparatuses from the Historical Collection of the Physics Instruments at University of
 131 Palermo.
 132

133 **Methods**

134 Thermogravimetry


135 Thermogravimetry (TG) experiments were carried out through a Q5000 IR apparatus (TA Instruments) under inert
 136 atmosphere. To this purpose, nitrogen flows of 25 and 10 cm³ min⁻¹ were used for the sample and the balance,
 137 respectively. The experiments were carried out by heating the sample (ca. 5 mg) from room temperature up to 600 °C.
 138 The heating rate (β) was systematically changed in order to investigate the kinetics of the non-isothermal degradation
 139 of the wooden historical materials through isoconversional methods. Specifically, five different heating rates (5, 10, 15,
 140 20 and 25 °C min⁻¹) were selected. As reported elsewhere (Blanco et al. 2014), the temperature calibration was
 141 conducted by using the Curie temperatures of proper standards (nickel, cobalt, and their alloys).

142

143

144

145 Fourier transform infrared (FTIR) spectroscopy

146 Fourier transform infrared (FTIR) measurements were performed at room temperature through a Frontier FTIR
147 spectrometer (PerkinElmer). The spectra were recorded in the range between 450 and 4000 cm^{-1} , while the spectral
148 resolution was set at 2 cm^{-1} . The experiments were conducted on KBr pellets with a low content (< 2 wt%) of milled
149 wooden sample. 

150

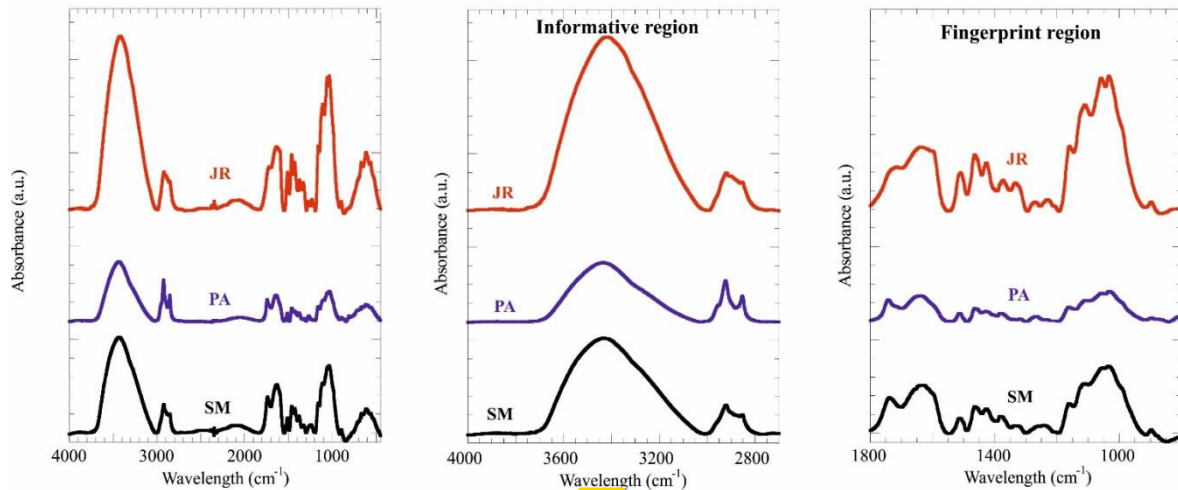
151

152
153
154
155
156
157

Results and discussion

FTIR spectroscopy

The analysis of FTIR spectra (Fig. 2) provided interesting insights on the composition and conservation state of the investigated wooden samples.



158
159
160

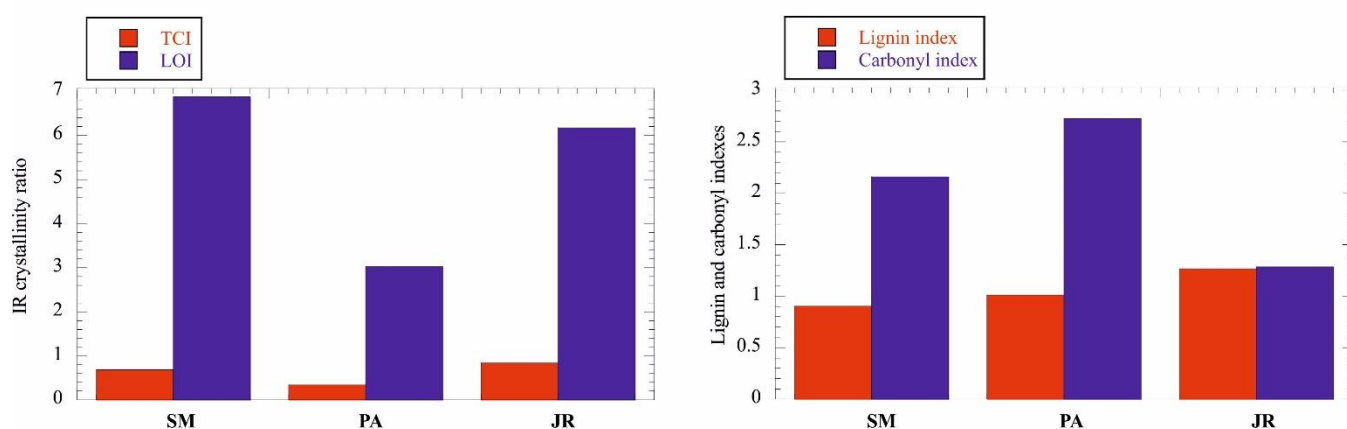
Fig. 2. FTIR spectra for the investigated wood samples.

As reported for Eucalyptus species (Carrillo-Varela et al. 2018), FTIR spectra of wooden materials are characterized by two regions on dependence of the wavelength range. As shown in Fig. 2, all the samples present a significant broad peak (centered at ca. 3400 cm⁻¹) in the “informative” region, which refers to the wavelength range between 4000 and 2700 cm⁻¹. This peak can be attributed to OH stretching vibration (Fengel 1992; Kondo 1997). Consequently, this signal can be related to the degree of hydrogen bonding between hydroxyl groups in wood components (cellulose, hemicellulose, lignin and water) (Církva et al. 2004; Popescu et al. 2011). Within the “informative” region, we detected a band at ca. 2900 cm⁻¹, which is due to asymmetric and symmetric CH stretching (Collier et al. 1997; Schwanninger et al. 2004). Generally, the absorption intensity at 2900 cm⁻¹ is used as internal standard for determination of the cellulose structural degree in wooden samples (Poletto et al. 2014; Odabas et al. 2016).

Within the wavelength range between 1800 and 800 cm⁻¹ (“fingerprint” region), we focused on the following signals characteristic of wood (Carrillo-Varela et al. 2018): 1) C=O stretching vibrations of carboxyl and acetyl groups in hemicellulose (peak centered at 1740 cm⁻¹) 2) C=C stretching of the aromatic ring in lignin (band at 1510 cm⁻¹); 3) CH₂ bending of cellulose (band at 1430 cm⁻¹); 4) CH bending in cellulose and hemicellulose (band at 1372 cm⁻¹); 5) C-H vibrational mode in cellulose (peak centered at 897 cm⁻¹). The quantitative analysis of the mentioned FTIR signals allowed us to determine specific indexes related to both the cellulose crystallinity and the composition of the wooden

176 samples. Regarding the cellulose crystallinity, we estimated the total crystalline index (TCI) by the ratio between the
 177 absorption intensities at 1372 and 2900 cm^{-1} . In addition, we calculated the lateral order index (LOI) by ratio between
 178 the bands at 1429 and 897 cm^{-1} . Fig. 3 compares the FTIR crystallinity indexes for the investigated wood samples. We
 179 detected that PA presents the lowest TCI and LOI values with respect to those of the other woods (SM and JR), which
 180 possess similar cellulose crystallinity. Based on these results, we can state that cellulose in PA exhibits the largest
 181 degree of disorder (Carrillo et al. 2004; Poletto et al. 2012).

182



183

184 **Fig. 3.** Relative crystallinity (TCI and LOI) and lignin/carbonyl indexes determined from the FTIR spectra analysis of
 185 the investigated wood samples.

186

187 Regarding the wood composition, we determined the lignin and carbonyl indexes as

188

$$189 \text{ Lignin index (L.I.)} = (I_{1510 \text{ cm}^{-1}})/(I_{1372 \text{ cm}^{-1}}) \quad (1)$$

$$190 \text{ Carbonyl index (C.I.)} = (I_{1740 \text{ cm}^{-1}})/(I_{1372 \text{ cm}^{-1}}) \quad (2)$$

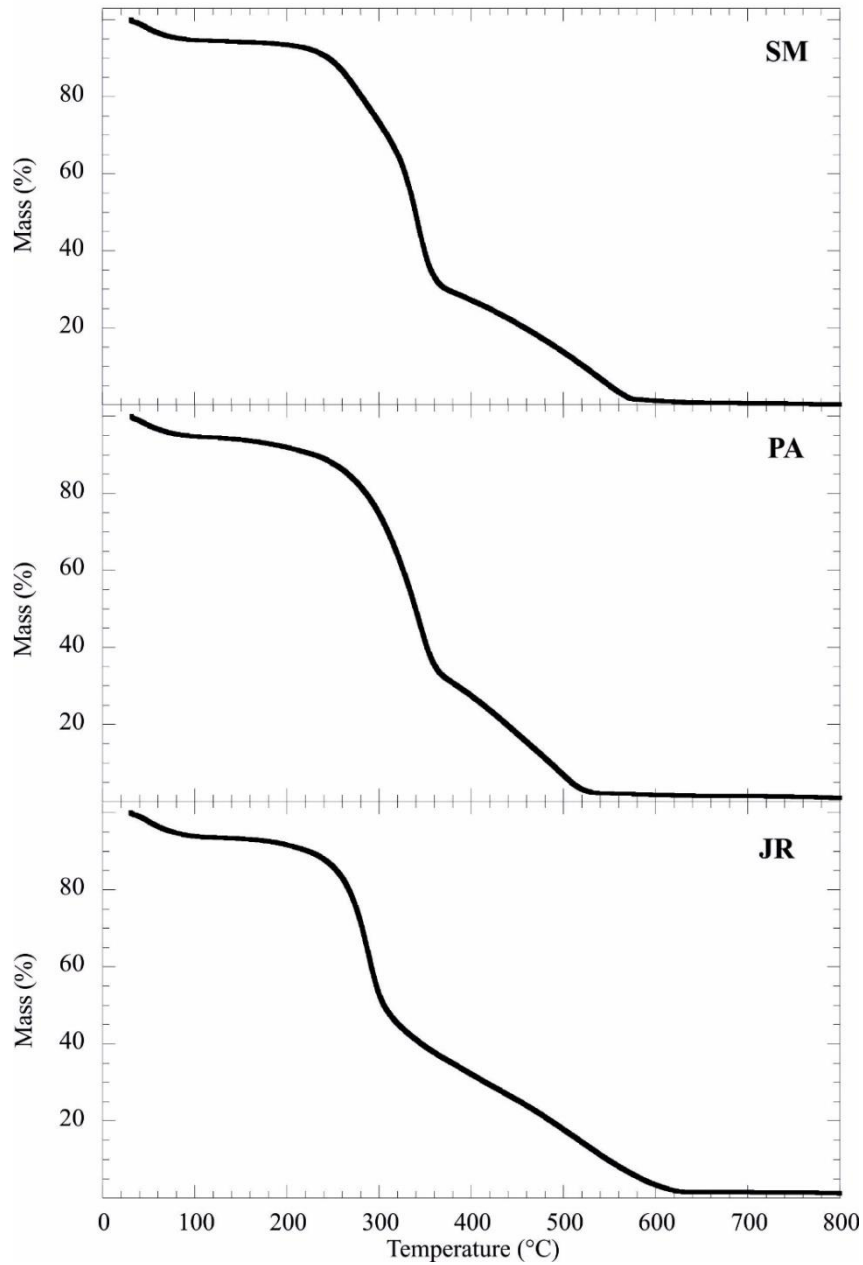
191

192 It should be noted that both indexes can be used to evaluate the conservation state of historical and archaeological
 193 woods (Gupta et al. 2015; Cavallaro et al. 2018). As evidenced by Fig. 3, the investigated wood samples possess
 194 different L.I. and C.I. values. We observed that C.I. and L.I. follow the trends PA > SM > JR and JR > PA > SM,
 195 respectively. These results highlight that the lignin contribution is not correlated with that of C=O groups.

196

197 Thermal properties

198 The thermal properties of the investigated wood samples were investigated by thermogravimetry. Fig. 4 shows the
 199 thermogravimetric curves (obtained at $\beta = 10 \text{ }^\circ\text{C min}^{-1}$) of the historical woods.



200

201 **Fig. 4.** Thermogravimetric curves of the wood samples.

202

203 As a general result, we observed three different mass losses that can be attributed to specific degradation processes of
 204 wooden materials. The several mass losses of each wood are collected in Table 2.

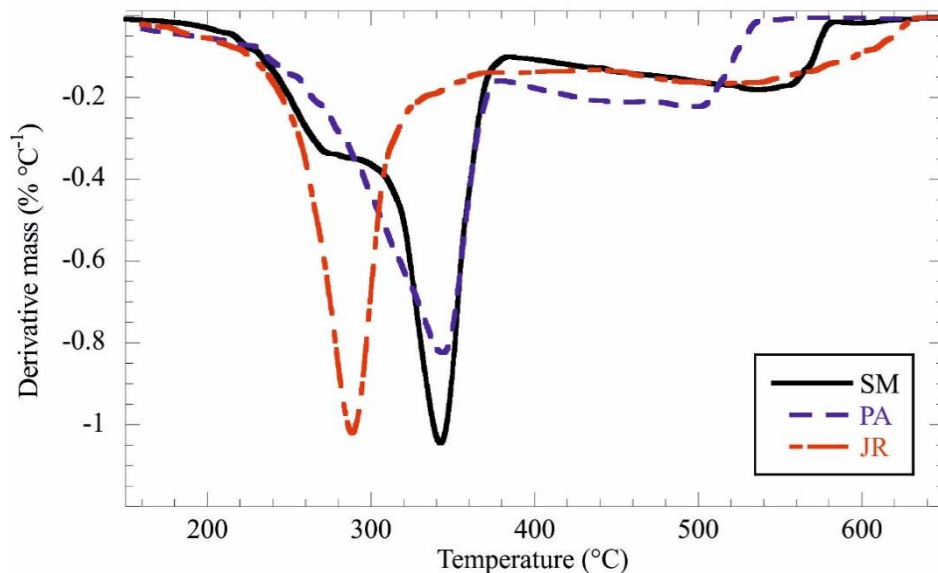
205

206 **Table 2.** Mass losses of the historical woods obtained by TG measurements at $\beta = 10 \text{ }^\circ\text{C min}^{-1}$

Wood	ML ₂₅₋₁₅₀ (wt%)	ML ₁₈₀₋₃₈₀ (wt%)	ML ₃₈₀₋₆₀₀ (wt%)	(ML ₁₈₀₋₃₈₀)/(ML ₃₈₀₋₆₀₀)	DTG peak ($^\circ\text{C}$)
SM	5.65 ± 0.06	64.6 ± 0.7	28.1 ± 0.3	0.435 ± 0.009	342 ± 3
PA	5.93 ± 0.06	62.0 ± 0.7	28.9 ± 0.3	0.46 ± 0.01	341 ± 3
JR	6.67 ± 0.07	57.6 ± 0.6	31.5 ± 0.3	0.54 ± 0.01	288 ± 3

207

208 The first degradation step takes place within the temperature range between 25 and 150 °C as a consequence of the
209 expulsion of the water molecules physically adsorbed into the wood structure. Accordingly, the mass loss at 25-150 °C
210 (ML_{25-150}) is correlated to the moisture content of the sample (Lisuzzo et al. 2019). As evidenced by Table 2, the largest
211 ML_{25-150} was detected for JR, which is the wood with the strongest hygroscopic degree.
212 As expected for the pyrolysis of lignocellulosic materials (Barneto et al. 2011), the historical woods mostly degraded
213 within the temperature interval between 180 and 600 °C (Fig. 3). In particular, we observed two separated mass losses
214 (at 180-380 and 380-600 °C) highlighting that the wood pyrolysis represents a multistep degradation mechanism.
215 Accordingly to literature (Cao et al. 2010; Barneto et al. 2011), the mass losses at 180-380 °C ($ML_{180-380}$) and 380-600
216 °C ($ML_{380-600}$) can be associated to the pyrolysis processes of the wood components, which are hemicellulose, cellulose
217 and lignin. Specifically, the depolymerization of hemicellulose and the cleavage of the glycosidic linkage of cellulose
218 occur between 180 and 380 °C, while lignin degrades in a wider temperature range (from 250 to 600 °C) (Kim et al.
219 2006). On this basis, the $(ML_{180-380})/(ML_{380-600})$ ratio could be correlated to the specific composition of the historical
220 wood. As shown in Table 2, the largest $(ML_{180-300})/(ML_{380-600})$ ratio was estimated for JR, while SM exhibited the
221 lowest value. These results are consistent with the lignin index data determined through FTIR spectroscopy. The
222 interpretation of the differential thermogravimetric (DTG) curves (Fig. 5) provided a more accurate description of the
223 wood pyrolysis.



224
225 **Fig. 5.** Differential thermogravimetric curves of the wood samples.
226

227 Within the first degradation step, all the samples evidenced a DTG peak that can be attributed to the cellulose
228 degradation. Compared to the other woods, a relevant reduction (ca. 60 °C) of the DTG peak temperature was observed
229 for JR. Namely, cellulose in JR exhibited the lowest thermal stability. In addition to the main peak, the DTG curve of

230 SM showed a shoulder at lower temperature (ca. 275 °C), which is due to the hemicellulose degradation. Similar
231 thermal behavior was observed in sapwood of *Pinus canariensis*, which was extensively used in the traditional Canarian
232 architecture (González-Díaz and Alonso-López 2017). Finally, all DTG curves exhibited a broad tail at higher
233 temperature (within the second degradation step) as a consequence of the lignin thermal decomposition.

234

235 **Kinetics of wood pyrolysis**

236 We investigated the kinetic aspects of the wood pyrolysis process by a non-isothermal thermogravimetric study based
237 on model free isoconversional methods, which include both integral and differential procedures (Vyazovkin et al. 2014;
238 Trache et al. 2017). To this purpose, thermogravimetric experiments at five different heating rates were conducted. The
239 data analyses were limited to the temperature interval between 180 and 380 °C, where the pyrolysis of all the wood
240 components occurs. Among the integral isoconversional procedures, the Kissinger–Akahira–Sunose (KAS) method
241 was selected. Literature reports that the KAS method is suitable to investigate the wood pyrolysis (Słopiecka et al.
242 2012; Azizi et al. 2017), the combustion reaction of low-rank coal char (Hu et al. 2018) and the thermal decomposition
243 of natural polymers (Makaremi et al. 2017; Bertolino et al. 2018). The KAS method can be expressed as

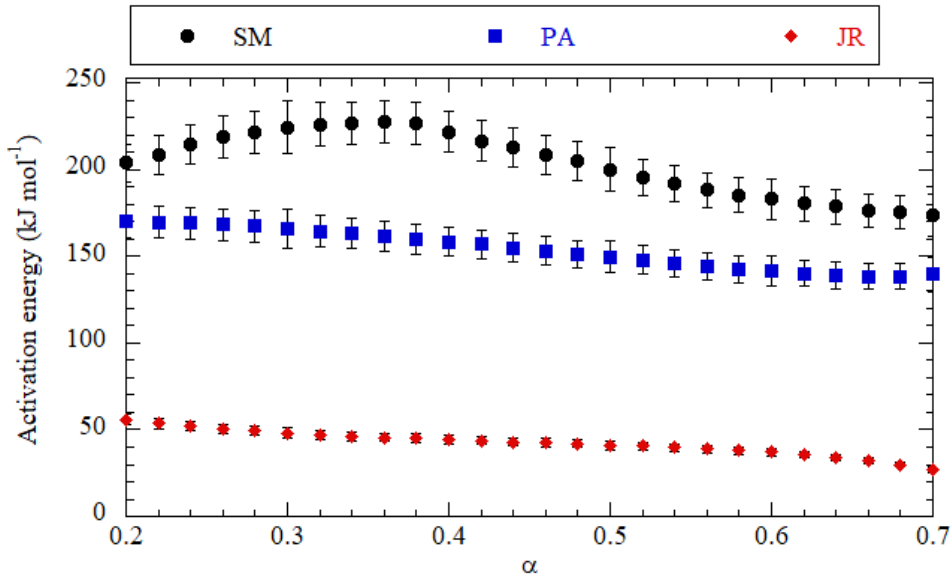
244

$$245 \ln(\beta/T^2) = \ln(AR/E_a g(\alpha)) - E_a/RT \quad (3)$$

246

247 where A and R are the pre-exponential factor and gas constant, respectively, while $g(\alpha)$ represents the integral
248 conversion function. According to equation 3, we can determine the activation energy (E_a) at each conversion degree
249 (α) by the slope of the $\ln(\beta/T^2)$ vs $1/T$ plot.

250 Fig. 6 shows the dependence of E_a on α for the pyrolysis of the investigated historical woods.



251

252 **Fig. 6.** KAS activation energy as a function of the conversion degree for the wood samples.

253

254 We observed that E_a is not significantly influenced by α (ranging between 0.2 and 0.7) for JR and PA, while a small
 255 peak (at $\alpha = 0.35$) was detected for SM. The latter might be related to the presence of hemicellulose evidenced by the
 256 shoulder in the DTG curve of SM wooden sample (Fig. 5). Interestingly, the historical woods exhibited different E_a
 257 values, which reflect variable kinetic properties in the pyrolysis of the wood components. We calculated that the
 258 average E_a values are 203, 156 and 43 kJ mol⁻¹ for SM, PA and JR, respectively. On this basis, we can state that JR
 259 possesses the lowest energetic barrier to the pyrolysis. These results agree with the DTG peak data (Table 2), which
 260 revealed that JR is the worst wood in terms of thermal stability under inert atmosphere. According to the TG data, we
 261 can assert that JR is the most sensitive wood to the decay and structural deterioration. Therefore, JR needs more
 262 accurate protocols for its preservation.

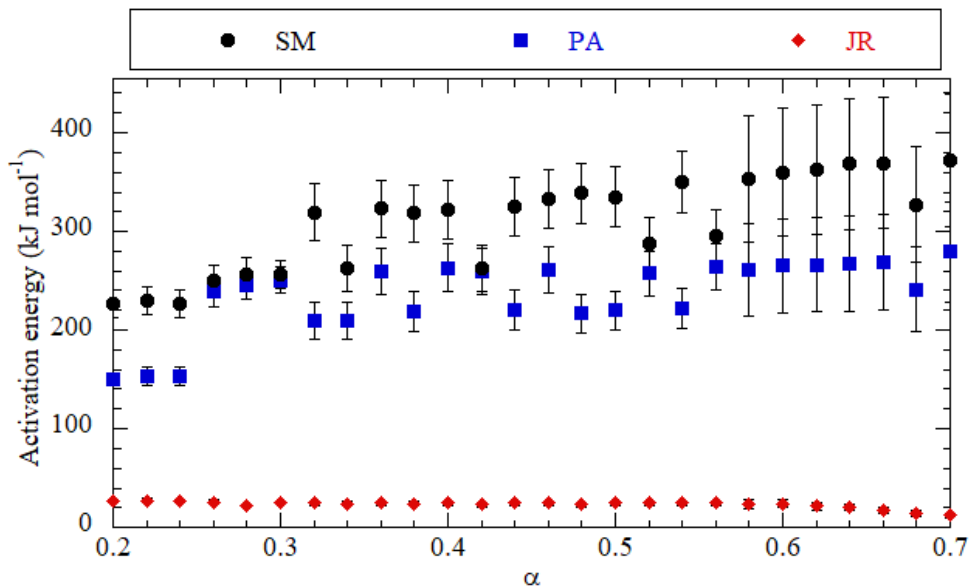
263 In addition to the KAS method, kinetic studies were carried out using the differential Friedman approach, which was
 264 successfully employed for the investigation of the pyrolysis processes in pinewood (Mishra et al. 2015), beechwood
 265 and flax shives (Abdelouahed et al. 2017). Furthermore, the Friedman method revealed as a suitable model free
 266 procedure for the kinetic analysis of the thermal decomposition of modified cellulose, such as methylcellulose
 267 (Bertolino et al. 2016) and hydroxypropylcellulose (Cavallaro et al. 2011b). The Friedman method is expressed by the
 268 following equation

269

$$270 \ln(\beta \cdot da/dT) = \ln(A \cdot f(\alpha)) - E_a/RT \quad (4)$$

271

272 where $f(\alpha)$ is a function of the conversion degree that is related to the reaction mechanism. Based on the equation 4, the
 273 specific slope of the $\ln(\beta \cdot da/dT)$ vs $1/T$ function provides E_a at variable α . The E_a vs α trends obtained by the
 274 Friedman equation are presented in Fig. 7.



275
 276 **Fig. 7.** Friedman activation energy as a function of the conversion degree for the wood samples.

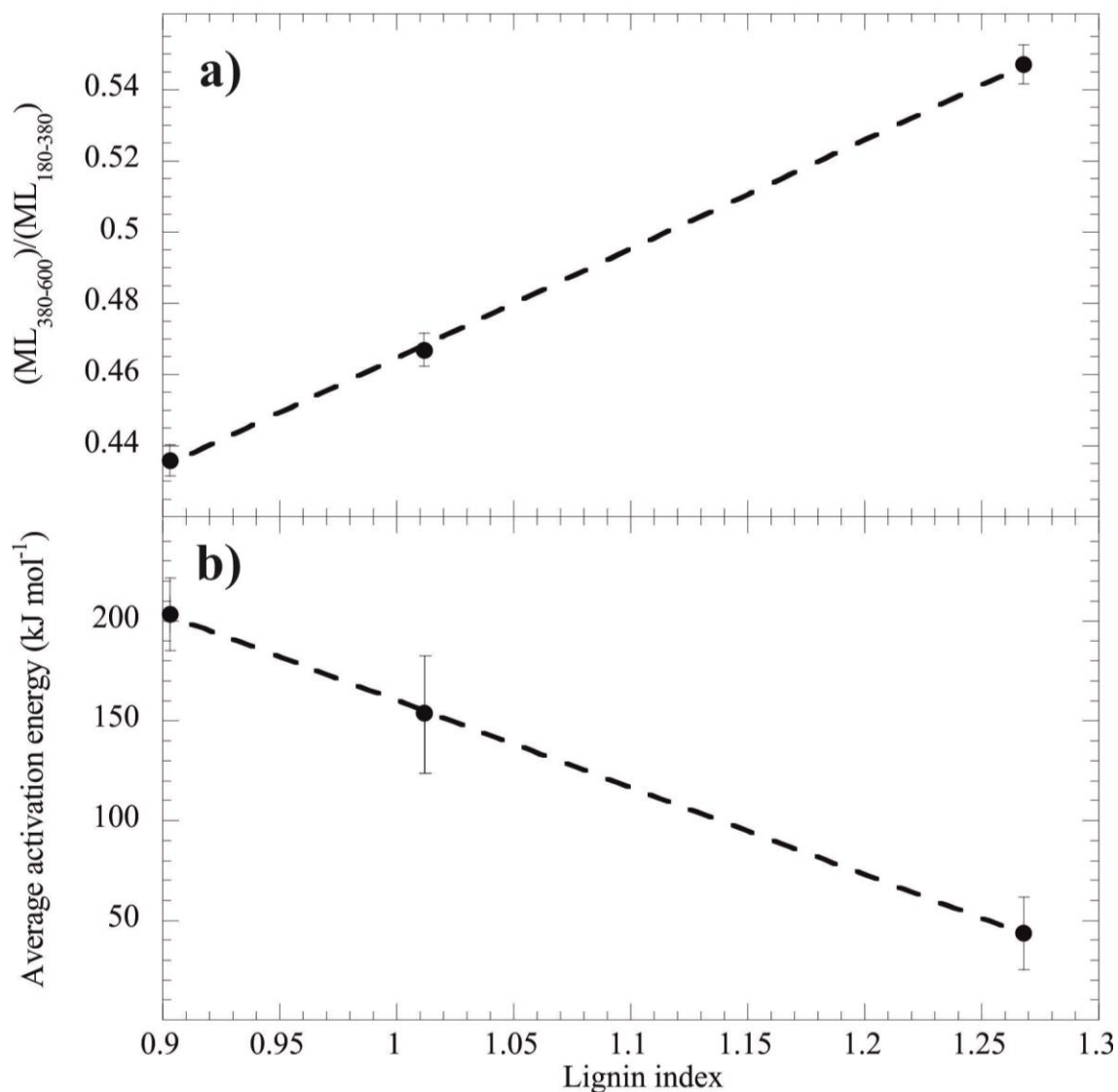
277
 278 Compared to the KAS method, we observed a higher level of fluctuations as well as larger errors on the E_a values
 279 indicating that the Friedman procedure provided less accurate results on the kinetics of pyrolysis of the historical
 280 woods. However, it should be noted that the Friedman analysis confirmed that JR is characterized by much lower E_a
 281 values with respect to those of SM and PA.

282
 283 **Correlation between thermal properties and FTIR spectroscopy**

284 As evidenced in the previous paragraphs, the thermogravimetric results can be properly interpreted on the basis of the
 285 wood composition obtained by the FTIR spectroscopy analysis. In this regards, Fig. 8 shows the influence of the lignin
 286 index on the thermogravimetric parameters, such as $(ML_{380-600})/(ML_{180-380})$ ratio and the average activation energy
 287 calculated through the KAS method.

288 As concerns the $(ML_{380-600})/(ML_{180-380})$ ratio, we observed a linear increase with the lignin index (Fig. 8a) confirming
 289 that the thermal degradation of the cellulosic components occurs at 180-380 °C, while lignin mostly decomposes in the
 290 temperature interval between 380 and 600 °C. Based on the linear fitting, we determined the following relation

291
 292
$$(ML_{380-600})/(ML_{180-380}) = (0.158 \pm 0.006) + (0.306 \pm 0.005) \cdot \text{L.I.} \quad (5)$$



294

295

296 **Fig. 8.** Dependence of the $(ML_{380-600})/(ML_{180-380})$ ratio (a) and KAS average activation energy (b) on the lignin index of
 297 the wood samples. The dashed lines represent the linear fitting according to equations 5 and 6.

298

299 According to equation 5, the lignin composition in the wooden samples might be indirectly estimated by
 300 thermogravimetric experiments. As highlighted by Fig. 8b, the average activation energy for the wood pyrolysis shows
 301 a decreasing linear trend with the lignin index. The linear regression of the E_a vs L.I. trend (Fig. 8b) allowed us to
 302 determine the following equation

303

$$304 \quad E_a = (596 \pm 7) - (436 \pm 6) \cdot \text{L.I.} \quad (6)$$

305 According to equation 6, we could predict the kinetics of the pyrolysis for wooden materials by considering their
 306 specific lignin index determined through FTIR spectroscopy.

307 It should be noted that equations 5,6 cannot be used as a general protocol for the thermal and structural characterization
308 of wooden materials. Nevertheless, the obtained functions demonstrated that thermogravimetric results can be
309 univocally interpreted by the analysis of the FTIR spectra of the woods. This consideration is remarkable being that the
310 investigated woods were employed in the manufacturing of physical apparatuses from XIX century. Therefore, the
311 combination of TGA and FTIR spectroscopy analyses might be useful to investigate the conservation state of wooden
312 artworks.

313

314

Conclusions

315 Historical woods from XIX century were characterized by thermogravimetry and FTIR spectroscopy. In detail, the
316 investigated samples refer to wood portions of apparatuses of the Historical Collection of the Physics Instruments at the
317 University of Palermo. In addition, the woods belong to different taxa (*Swietenia mahagoni*, *Picea abies* and *Juglans*
318 *regia*), which were extensively used for the fabrication of physics instruments during XIX century.

319 According to their different taxon, the woods exhibited variable lignin and carbonyl indexes as well peculiar cellulose
320 crystallinity degree. In this regards, we detected that cellulose in *Picea abies* possesses the highest degree of disorder.

321 As concerns the thermal properties, we investigated the wood pyrolysis by performing thermogravimetric
322 measurements under inert atmosphere. The analysis of both thermogravimetric and differential thermogravimetric
323 curves evidenced that the historical woods present different thermal stability depending on their structural and
324 compositional characteristics. Compared to the other woods, we observed that *Juglans regia* exhibits a strong reduction
325 (ca. 60 °C) of the cellulose degradation temperature. This result was supported by the non-isothermal
326 thermogravimetric studies, which evidenced that the activation energy of the wood pyrolysis for *Juglans regia* is ca. 4-
327 5 times lower than those of the other wooden samples. On this basis, we can state that *Juglans regia* is the most
328 sensitive wood to the structural deterioration. The thermal properties of the historical woods were correlated to the
329 specific indexes estimated from FTIR spectra. Interestingly, we observed that the activation energy of the pyrolysis
330 process linearly decreases with the lignin index of the wood.

331 In conclusion, this work evidenced that the combination of FTIR spectroscopy and thermogravimetric analysis can
332 provide a robust protocol to predict the conservation state of historical woods with variable structural and thermal
333 characteristics.

334

335

Acknowledgment

336 The work was financially supported by Progetto di ricerca e sviluppo "AGM for CuHe" (ARS01_00697) and
337 University of Palermo FFR project MODIFY. The authors have no conflicts of interest to declare.

338
339
340
341
342
343
344
345
346
347
348
349
350
351
352
353
354
355
356
357
358
359
360
361
362

References

- Abdelouahed L, Leveneur S, Vernieres-Hassimi L, et al (2017) Comparative investigation for the determination of kinetic parameters for biomass pyrolysis by thermogravimetric analysis. *J Therm Anal Calorim* 129:1201–1213. doi: 10.1007/s10973-017-6212-9
- Agliolo Gallitto A., Chinnici I., Bartolone F. (2017) Collezione Storica degli Strumenti di Fisica: Catalogo degli strumenti di Acustica. Università degli Studi di Palermo, Palermo. ISBN 978-88-941245-2-1
- Agliolo Gallitto A., Chinnici I., Bartolone F. (2018) The Collection of historical instruments of Acoustics of the University of Palermo, *Museologia Scientifica* 12:48-54
- Azizi K, Keshavarz Moraveji M, Abedini Najafabadi H (2017) Characteristics and kinetics study of simultaneous pyrolysis of microalgae *Chlorella vulgaris*, wood and polypropylene through TGA. *Bioresour Technol* 243:481–491. doi: 10.1016/j.biortech.2017.06.155
- Bardet M, Foray MF, Trân Q-K (2002) High-Resolution Solid-State CPMAS NMR Study of Archaeological Woods. *Anal Chem* 74:4386–4390. doi: 10.1021/ac020145j
- Barneto AG, Vila C, Ariza J, Vidal T (2011) Thermogravimetric measurement of amorphous cellulose content in flax fibre and flax pulp. *Cellulose* 18:17–31. doi: 10.1007/s10570-010-9472-0
- Bertolino V, Cavallaro G, Lazzara G, et al (2018) Halloysite nanotubes sandwiched between chitosan layers: Novel bionanocomposites with multilayer structures. *New J Chem* 42:8384–8390. doi: 10.1039/c8nj01161c
- Bertolino V, Cavallaro G, Lazzara G, et al (2016) Effect of the Biopolymer Charge and the Nanoclay Morphology on Nanocomposite Materials. *Ind Eng Chem Res* 55:7373–7380. doi: 10.1021/acs.iecr.6b01816
- Blanco I, Abate L, Bottino FA, Bottino P (2014) Thermal behaviour of a series of novel aliphatic bridged polyhedral oligomeric silsesquioxanes (POSSs)/polystyrene (PS) nanocomposites: The influence of the bridge length on the resistance to thermal degradation. *Polym Degrad Stab* 102:132–137. doi: 10.1016/j.polymdegradstab.2014.01.029
- Blanco I, Cicala G, Latteri A, et al (2017) Thermal characterization of a series of lignin-based polypropylene blends. *J Therm Anal Calorim* 127:147–153. doi: 10.1007/s10973-016-5596-2

- 363 Borysiak S (2013) Fundamental studies on lignocellulose/polypropylene composites: Effects of wood treatment on the
364 transcrySTALLINE morphology and mechanical properties. *J Appl Polym Sci* 127:1309–1322. doi:
365 10.1002/app.37651
- 366 Broda M, Mazela B, Dutkiewicz A (2019) Organosilicon compounds with various active groups as consolidants for the
367 preservation of waterlogged archaeological wood. *J Cult Herit* 35:123–128. doi: 10.1016/j.culher.2018.06.006
- 368 Broda M, Popescu C-M (2019) Natural decay of archaeological oak wood versus artificial degradation processes — An
369 FT-IR spectroscopy and X-ray diffraction study. *Spectrochim Acta A Mol Biomol Spectrosc* 209:280–287.
370 doi: 10.1016/j.saa.2018.10.057
- 371 Budrugaec P, Segal E, Perez-Maqueda LA, Criado JM (2004) The use of the IKP method for evaluating the kinetic
372 parameters and the conversion function of the thermal dehydrochlorination of PVC from non-isothermal data.
373 *Polym Degrad Stab* 84:311–320. doi: doi: 10.1016/j.polymdegradstab.2004.01.017
- 374 Budrugaec P (2018) A simple and precise differential incremental isoconversional method to kinetic analysis of
375 heterogeneous processes under arbitrary temperature programs. *Thermochim Acta* 661:116–123. doi:
376 10.1016/j.tca.2018.01.025
- 377 Bugg TD, Ahmad M, Hardiman EM, Singh R (2011) The emerging role for bacteria in lignin degradation and bio-
378 product formation. *Curr Opin Biotechnol* 22:394–400. doi: 10.1016/j.copbio.2010.10.009
- 379 Cao J, Tan Y, Che Y, Xin H (2010) Novel complex gel beads composed of hydrolyzed polyacrylamide and chitosan:
380 An effective adsorbent for the removal of heavy metal from aqueous solution. *Bioresour Technol* 101:2558–
381 2561. doi: 10.1016/j.biortech.2009.10.069
- 382 Carrillo F, Colom X, Suñol JJ, Saurina J (2004) Structural FTIR analysis and thermal characterisation of lyocell and
383 viscose-type fibres. *Eur Polym J* 40:2229–2234. doi: 10.1016/j.eurpolymj.2004.05.003
- 384 Carrillo I, Mendonça RT, Ago M, Rojas OJ (2018) Comparative study of cellulosic components isolated from different
385 Eucalyptus species. *Cellulose* 25:1011–1029. doi: 10.1007/s10570-018-1653-2
- 386 Carrillo-Varela I, Pereira M, Mendonça RT (2018) Determination of polymorphic changes in cellulose from Eucalyptus
387 spp. fibres after alkalization. *Cellulose* 25:6831–6845. doi: 10.1007/s10570-018-2060-4

- 388 Casdorff K, Keplinger T, Burgert I (2017) Nano-mechanical characterization of the wood cell wall by AFM studies:
389 comparison between AC- and QI™ mode. *Plant Methods* 13:60–60. doi: 10.1186/s13007-017-0211-5
- 390 Cavallaro G, Donato DI, Lazzara G, Milioto S (2011a) A comparative thermogravimetric study of waterlogged
391 archaeological and sound woods. *J Therm Anal Calorim* 104:451–457. doi: 10.1007/s10973-010-1229-3
- 392 Cavallaro G, Donato DI, Lazzara G, Milioto S (2011b) Films of Halloysite Nanotubes Sandwiched between Two
393 Layers of Biopolymer: From the Morphology to the Dielectric, Thermal, Transparency, and Wettability
394 Properties. *J Phys Chem C* 115:20491–20498. doi: 10.1021/jp207261r
- 395 Cavallaro G, Lazzara G, Milioto S, et al (2017) Nanocomposites based on esterified colophony and halloysite clay
396 nanotubes as consolidants for waterlogged archaeological woods. *Cellulose* 24:3367–3376. doi:
397 10.1007/s10570-017-1369-8
- 398 Cavallaro G, Milioto S, Parisi F, Lazzara G (2018) Halloysite Nanotubes Loaded with Calcium Hydroxide: Alkaline
399 Fillers for the Deacidification of Waterlogged Archeological Woods. *ACS Appl Mater Interfaces* 10:27355–
400 27364. doi: 10.1021/acsami.8b09416
- 401 Církva V, Polák R, Paleta O, et al (2004) Novel perfluoroalkylated derivatives of d-galactopyranose and xylitol for
402 biomedical uses. Hemocompatibility and effect on perfluorocarbon emulsions. *Carbohydr Res* 339:2177–2185.
403 doi: 10.1016/j.carres.2004.06.019
- 404 Collier W, Kalasinski F, Schulz TP (1997) Infrared study of lignin: assignment of methoxyl C–H bending and
405 stretching bands. *Holzforschung* 51:167–168. doi: 10.1515/hfsg.1997.51.2.167
- 406 Dedic D, Iversen T, Ek M (2013) Cellulose degradation in the Vasa: The role of acids and rust. *Stud Conserv* 58:308–
407 313. doi: 10.1179/2047058412Y.0000000069
- 408 Emmanuel V, Odile B, Céline R (2015) FTIR spectroscopy of woods: A new approach to study the weathering of the
409 carving face of a sculpture. *Spectrochim Acta A Mol Biomol Spectrosc* 136:1255–1259. doi:
410 10.1016/j.saa.2014.10.011
- 411 Fengel D (1992) Characterization of Cellulose by Deconvoluting the OH Valency Range in FTIR Spectra.
412 *Holzforschung* 46:283–288. doi: 10.1515/hfsg.1992.46.4.283

- 413 Giorgi R, Chelazzi D, Baglioni P (2005) Nanoparticles of Calcium Hydroxide for Wood Conservation. The
414 Deacidification of the Vasa Warship. *Langmuir* 21:10743–10748. doi: 10.1021/la0506731
- 415 Girometta C, Zeffiro A, Malagodi M, et al (2017) Pretreatment of alfalfa stems by wood decay fungus *Perenniporia*
416 *meridionalis* improves cellulose degradation and minimizes the use of chemicals. *Cellulose* 24:3803–3813.
417 doi: 10.1007/s10570-017-1395-6
- 418 González-Díaz E, Alonso-López J-M (2017) Characterization by thermogravimetric analysis of the wood used in
419 Canary architectural heritage. *J Cult Herit* 23:111–118. doi: 10.1016/j.culher.2016.09.002
- 420 Guo C, Song Y, Wang Q, Shen C (2006) Dynamic-mechanical analysis and SEM morphology of wood
421 flour/polypropylene composites. *J For Res* 17:315–318. doi: 10.1007/s11676-006-0072-7
- 422 Gupta BS, Jelle BP, Gao T (2015) Wood facade materials ageing analysis by FTIR spectroscopy. *Constr Mater*
423 168:219–231. doi: 10.1680/coma.13.00021
- 424 Hu Y, Wang Z, Cheng X, Ma C (2018) Non-isothermal TGA study on the combustion reaction kinetics and mechanism
425 of low-rank coal char. *RSC Adv* 8:22909–22916. doi: 10.1039/C8RA02618A
- 426 Iwamoto S, Saito Y, Yagishita T, et al (2019) Role of moisture in esterification of wood and stability study of ultrathin
427 lignocellulose nanofibers. *Cellulose* 26:4721–4729. doi: 10.1007/s10570-019-02408-x
- 428 Janković B (2014) The pyrolysis process of wood biomass samples under isothermal experimental conditions—energy
429 density considerations: application of the distributed apparent activation energy model with a mixture of
430 distribution functions. *Cellulose* 21:2285–2314. doi: 10.1007/s10570-014-0263-x
- 431 Kim H-S, Kim S, Kim H-J, Yang H-S (2006) Thermal properties of bio-flour-filled polyolefin composites with different
432 compatibilizing agent type and content. *Thermochim Acta* 451:181–188. doi: 10.1016/j.tca.2006.09.013
- 433 Kondo T (1997) The assignment of IR absorption bands due to free hydroxyl groups in cellulose. *Cellulose* 4:281–292.
434 doi: 10.1023/A:1018448109214
- 435 Lin W, Huang Y, Li J, et al (2018) Preparation of highly hydrophobic and anti-fouling wood using
436 poly(methylhydrogen)siloxane. *Cellulose* 25:7341–7353. doi: 10.1007/s10570-018-2074-y

437 Lisuzzo L, Cavallaro G, Pasbakhsh P, et al (2019) Why does vacuum drive to the loading of halloysite nanotubes? The
438 key role of water confinement. *J Colloid Interface Sci* 547:361–369. doi: 10.1016/j.jcis.2019.04.012

439 Makaremi M, Pasbakhsh P, Cavallaro G, et al (2017) Effect of Morphology and Size of Halloysite Nanotubes on
440 Functional Pectin Bionanocomposites for Food Packaging Applications. *ACS Appl Mater Interfaces* 9:17476–
441 17488. doi: 10.1021/acsami.7b04297

442 Mishra G, Kumar J, Bhaskar T (2015) Kinetic studies on the pyrolysis of pinewood. *Bioresour Technol* 182:282–288.
443 doi: 10.1016/j.biortech.2015.01.087

444 Mohomane SM, Motaung TE, Revaprasadu N (2017) Thermal Degradation Kinetics of Sugarcane Bagasse and Soft
445 Wood Cellulose. *Materials* 10:. doi: 10.3390/ma10111246

446 Moise V, Stanculescu I, Vasilca S, et al (2019) Consolidation of very degraded cultural heritage wood artefacts using
447 radiation curing of polyester resins. *Radiat Phys Chem* 156:314–319. doi: 10.1016/j.radphyschem.2018.11.028

448 Notley SM, Wågberg L (2005) Morphology of Modified Regenerated Model Cellulose II Surfaces Studied by Atomic
449 Force Microscopy: Effect of Carboxymethylation and Heat Treatment. *Biomacromolecules* 6:1586–1591. doi:
450 10.1021/bm050005u

451 Odabas N, Amer H, Bacher M, et al (2016) Properties of Cellulosic Material after Cationization in Different Solvents.
452 *ACS Sustain Chem Eng* 4:2295–2301. doi: 10.1021/acssuschemeng.5b01752

453 Poggi G, Toccafondi N, Melita LN, et al (2014) Calcium hydroxide nanoparticles for the conservation of cultural
454 heritage: new formulations for the deacidification of cellulose-based artifacts. *Appl Phys A* 114:685–693. doi:
455 10.1007/s00339-013-8172-7

456 Poletto M, Ornaghi HL, Zattera AJ (2014) Native Cellulose: Structure, Characterization and Thermal Properties.
457 *Materials* 7:6105–6119. doi: 10.3390/ma7096105

458 Poletto M, Zattera AJ, Santana RMC (2012) Structural differences between wood species: Evidence from chemical
459 composition, FTIR spectroscopy, and thermogravimetric analysis. *J Appl Polym Sci* 126:E337–E344. doi:
460 10.1002/app.36991

461 Popescu C-M, Popescu M-C, Singurel G, et al (2007) Spectral Characterization of Eucalyptus Wood. *Appl Spectrosc*
462 61:1168–1177. doi: 10.1366/000370207782597076

463 Popescu M-C, Popescu C-M, Lisa G, Sakata Y (2011) Evaluation of morphological and chemical aspects of different
464 wood species by spectroscopy and thermal methods. *J Mol Struct* 988:65–72. doi:
465 10.1016/j.molstruc.2010.12.004

466 Rasmussen H, Tanner D, Sorensen HR, Meyer AS (2017) New degradation compounds from lignocellulosic biomass
467 pretreatment: routes for formation of potent oligophenolic enzyme inhibitors. *Green Chem* 19:464–473. doi:
468 10.1039/C6GC01809B

469 Rotaru A (2016) Discriminating within the kinetic models for heterogeneous processes of materials by employing a
470 combined procedure under TKS-SP 2.0 software. *J Therm Anal Calorim* 126:919–932. doi: 10.1007/s10973-
471 016-5584-6

472 Rotaru A (2017) Thermal and kinetic study of hexagonal boric acid versus triclinic boric acid in air flow. *J Therm Anal*
473 *Calorim* 127:755–763. doi: 10.1007/s10973-016-5583-7

474 Schwanninger M, Rodrigues JC, Pereira H, Hinterstoisser B (2004) Effects of short-time vibratory ball milling on the
475 shape of FT-IR spectra of wood and cellulose. *Vib Spectrosc* 36:23–40. doi: 10.1016/j.vibspec.2004.02.003

476 Sebio-Puñal T, Naya S, López-Beceiro J, et al (2012) Thermogravimetric analysis of wood, holocellulose, and lignin
477 from five wood species. *J Therm Anal Calorim* 109:1163–1167. doi: 10.1007/s10973-011-2133-1

478 Słopiecka K, Bartocci P, Fantozzi F (2012) Thermogravimetric analysis and kinetic study of poplar wood pyrolysis.
479 *Appl Energy* 97:491–497. doi: 10.1016/j.apenergy.2011.12.056

480 Trache D, Abdelaziz A, Siouani B (2017) A simple and linear isoconversional method to determine the pre-exponential
481 factors and the mathematical reaction mechanism functions. *J Therm Anal Calorim* 128:335–348. doi:
482 10.1007/s10973-016-5962-0

483 Vyazovkin S, Chrissafis K, Di Lorenzo ML, et al (2014) ICTAC Kinetics Committee recommendations for collecting
484 experimental thermal analysis data for kinetic computations. *Thermochim Acta* 590:1–23. doi:
485 10.1016/j.tca.2014.05.036

486 Walsh Z, Janeček E-R, Jones M, Scherman OA (2017) Natural polymers as alternative consolidants for the preservation
487 of waterlogged archaeological wood. *Stud Conserv* 62:173–183. doi: 10.1179/2047058414Y.0000000149

488 Žlahtič Zupanc M, Mikac U, Serša I, et al (2019) Water distribution in wood after short term wetting. Cellulose 26:703–
489 721. doi: 10.1007/s10570-018-2102-y

490

491

492

493

494

495

496

497

498

499

500

501

502

503

504

505

506

507

508

509

510

511

512

513

514

515

516

517

518

Figs. captions

519

520 **Fig. 1.** Photos of the physics apparatuses from the Historical Collection of the Physics Instruments at University of
521 Palermo.

522 **Fig. 2.** FTIR spectra for the investigated wood samples.

523 **Fig. 3.** Relative crystallinity (TCI and LOI) and lignin/carbonyl indexes determined from the FTIR spectra analysis of
524 the investigated wood samples.

525 **Fig. 4.** Thermogravimetric curves of the wood samples.

526 **Fig. 5.** Differential thermogravimetric curves of the wood samples.

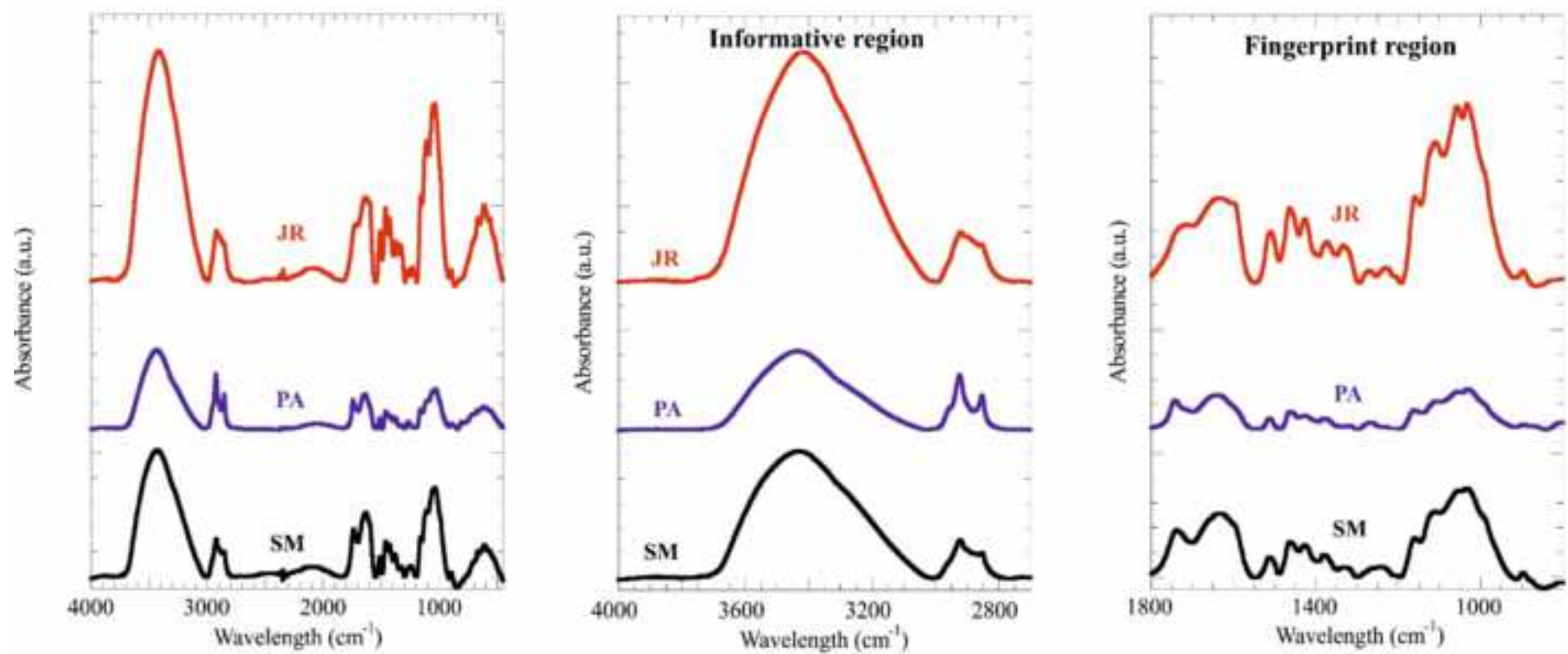
527 **Fig. 6.** KAS activation energy as a function of the conversion degree for the wood samples.

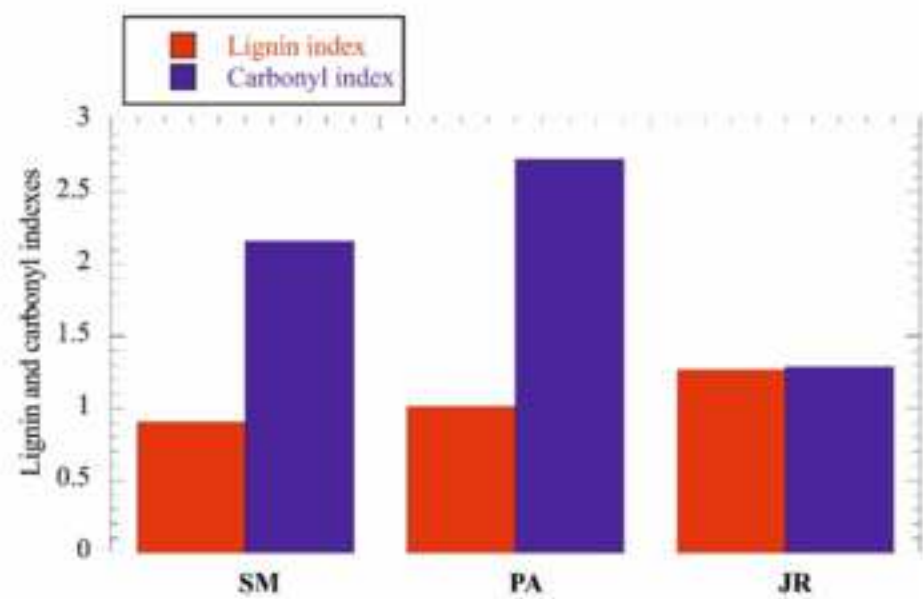
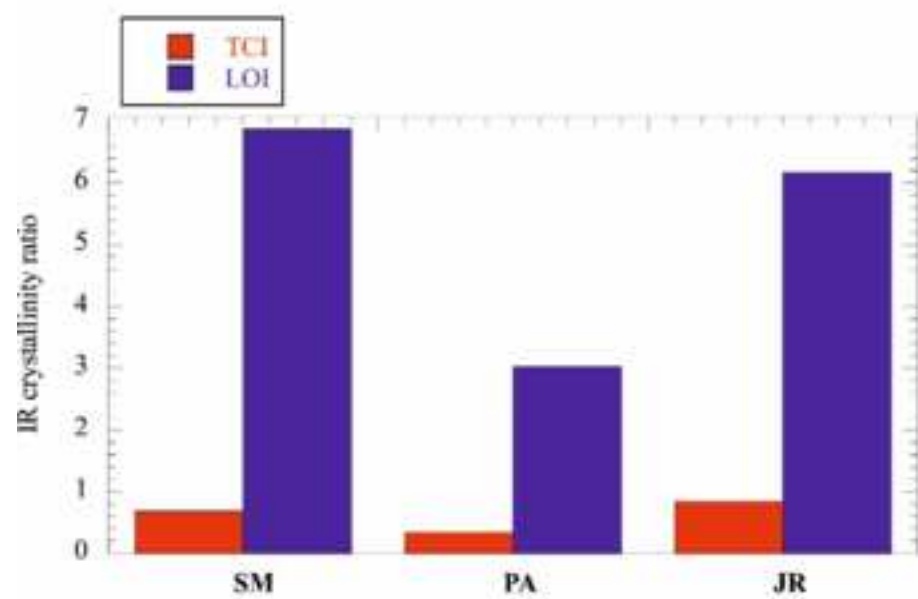
528 **Fig. 7.** Friedman activation energy as a function of the conversion degree for the wood samples.

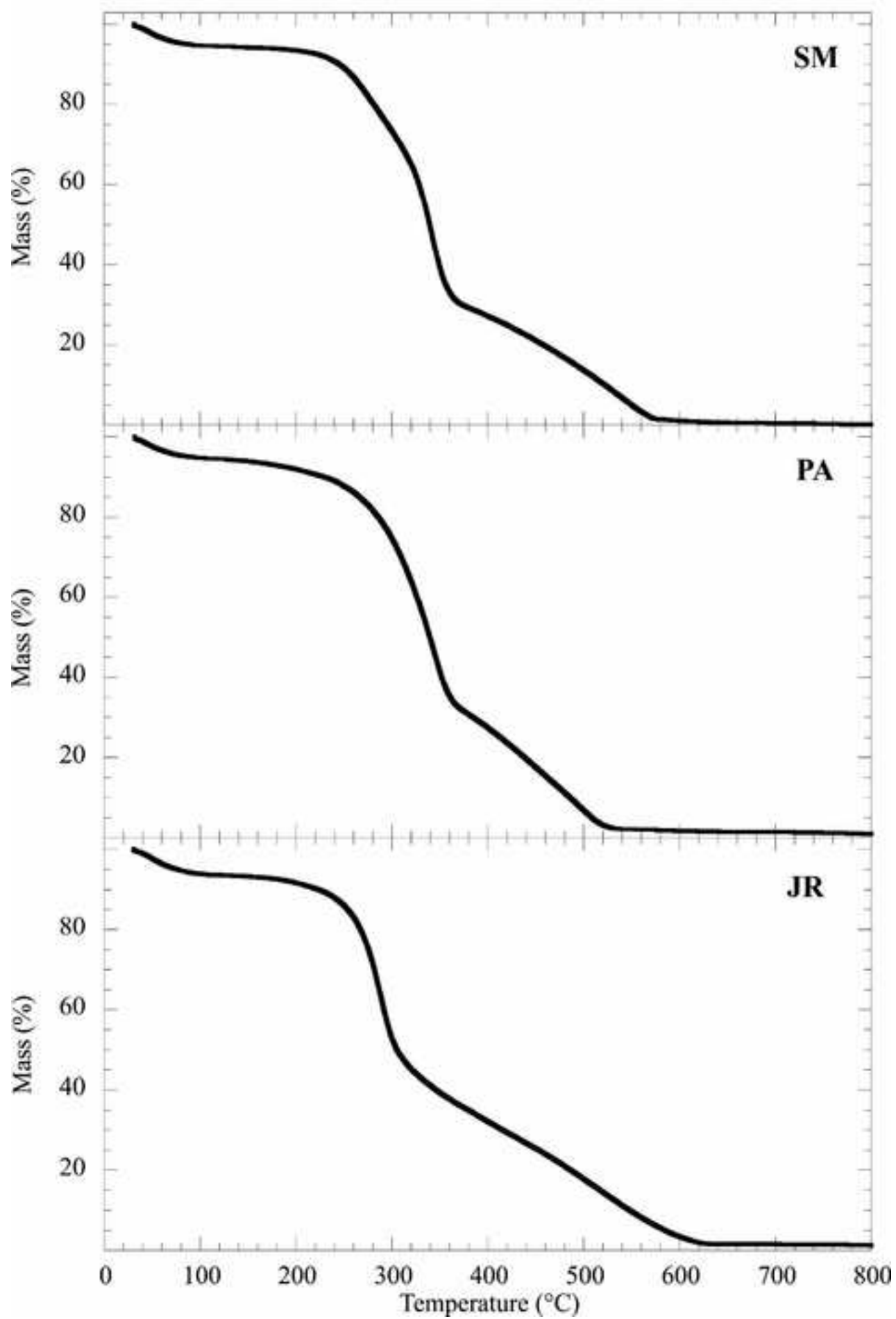
529 **Fig. 8.** Dependence of the (ML380-600)/(ML180-380) ratio (a) and KAS average activation energy (b) on the lignin
530 index of the wood samples. The dashed lines represent the linear fitting according to equations 5 and 6.

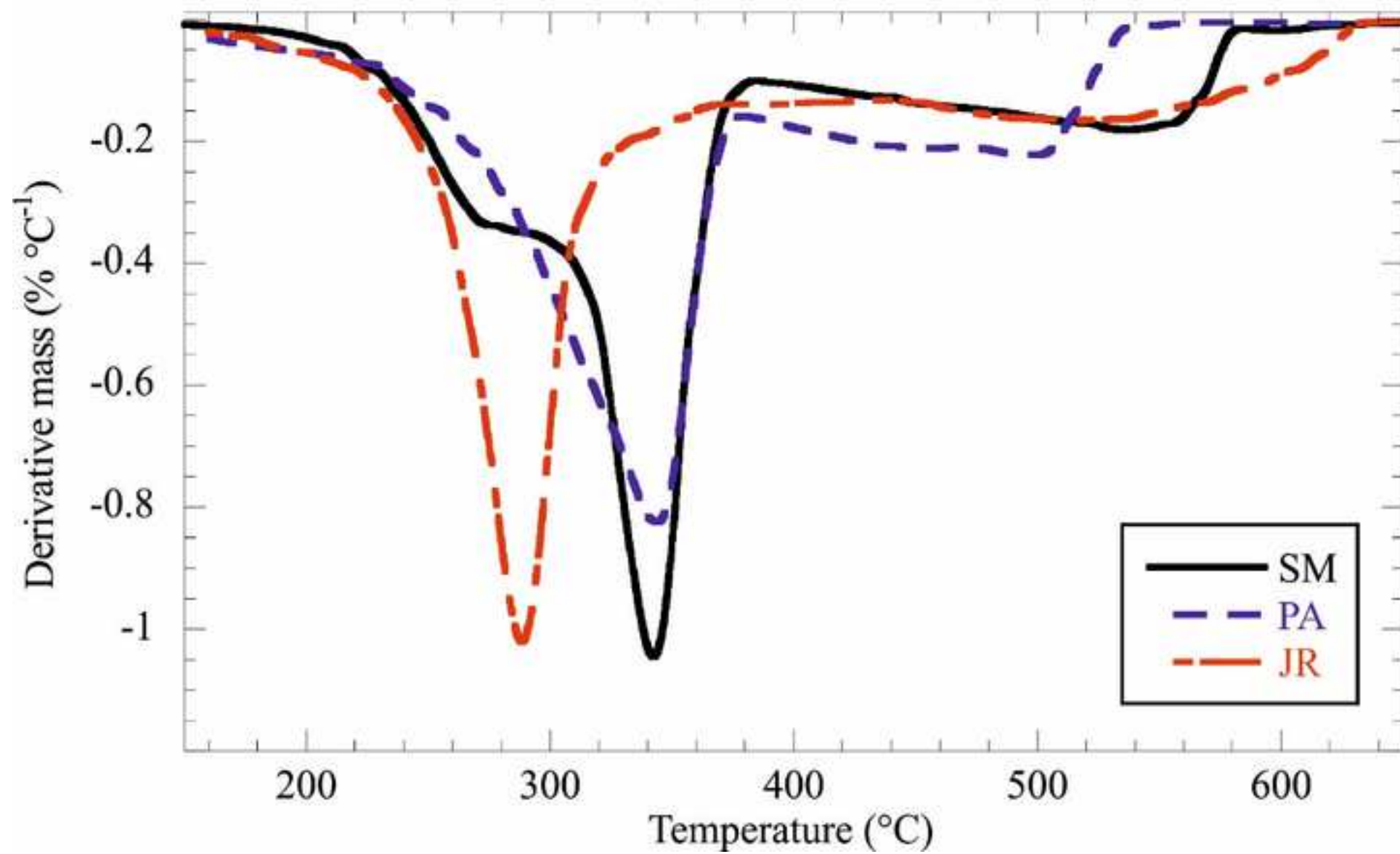
531

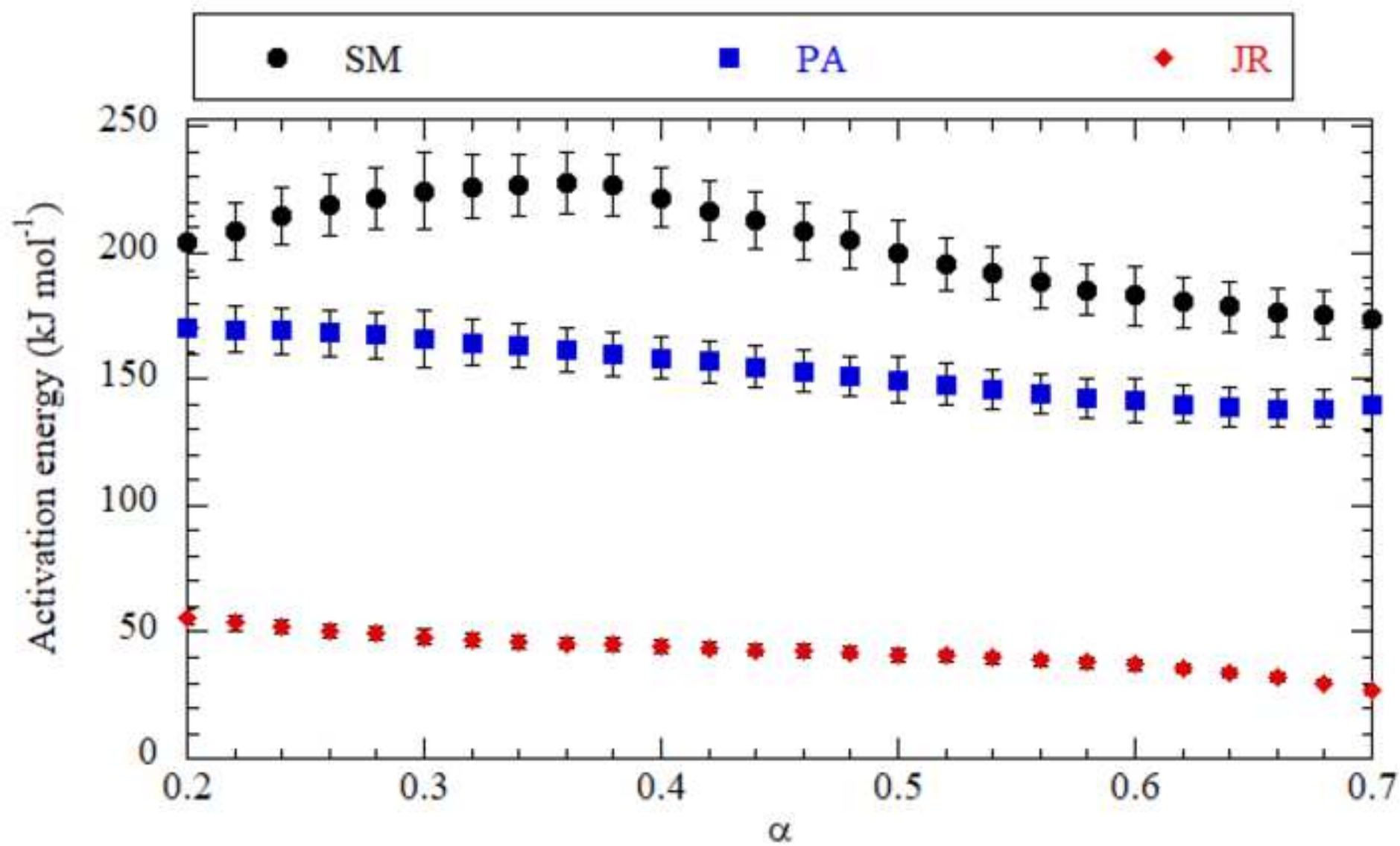


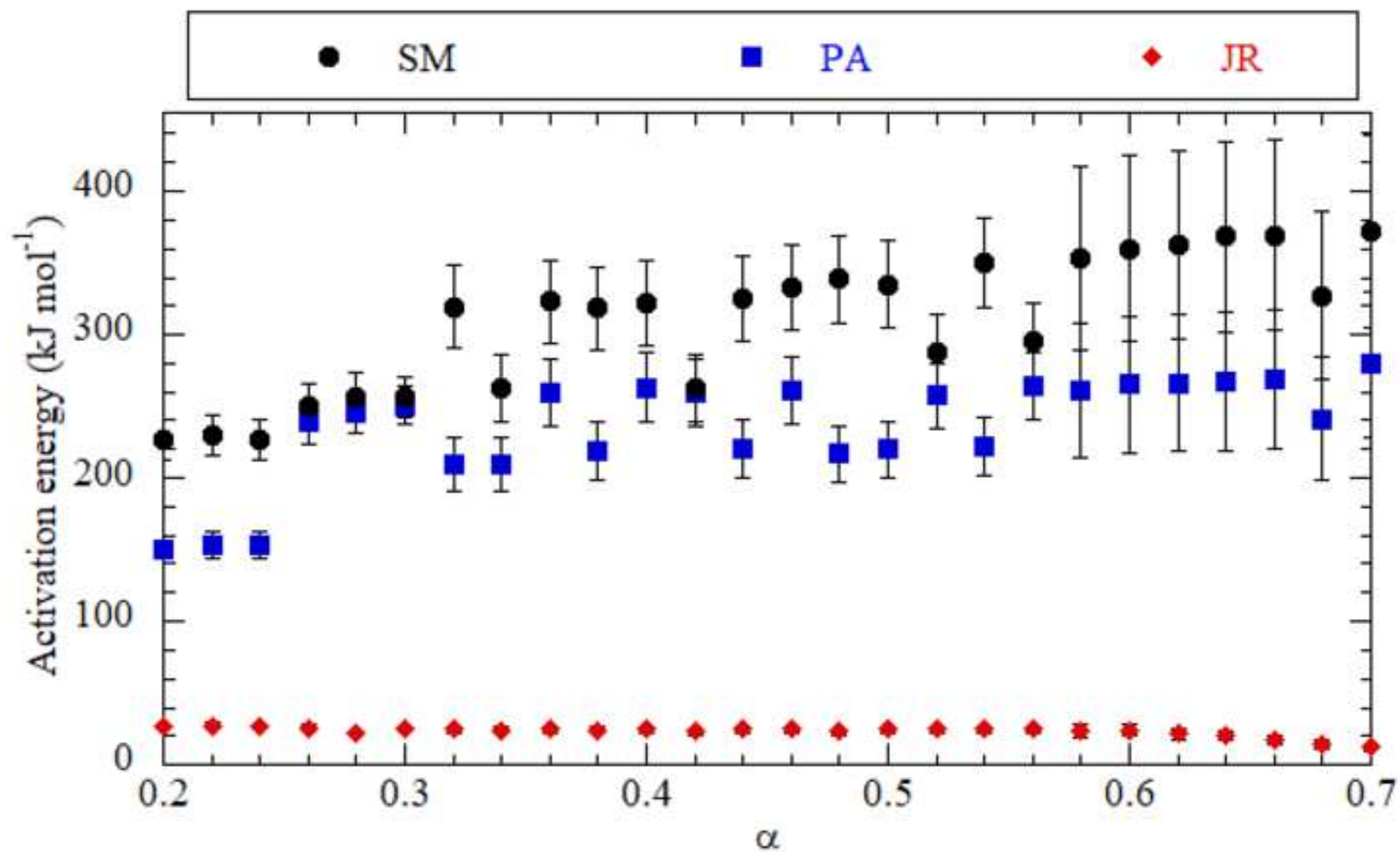












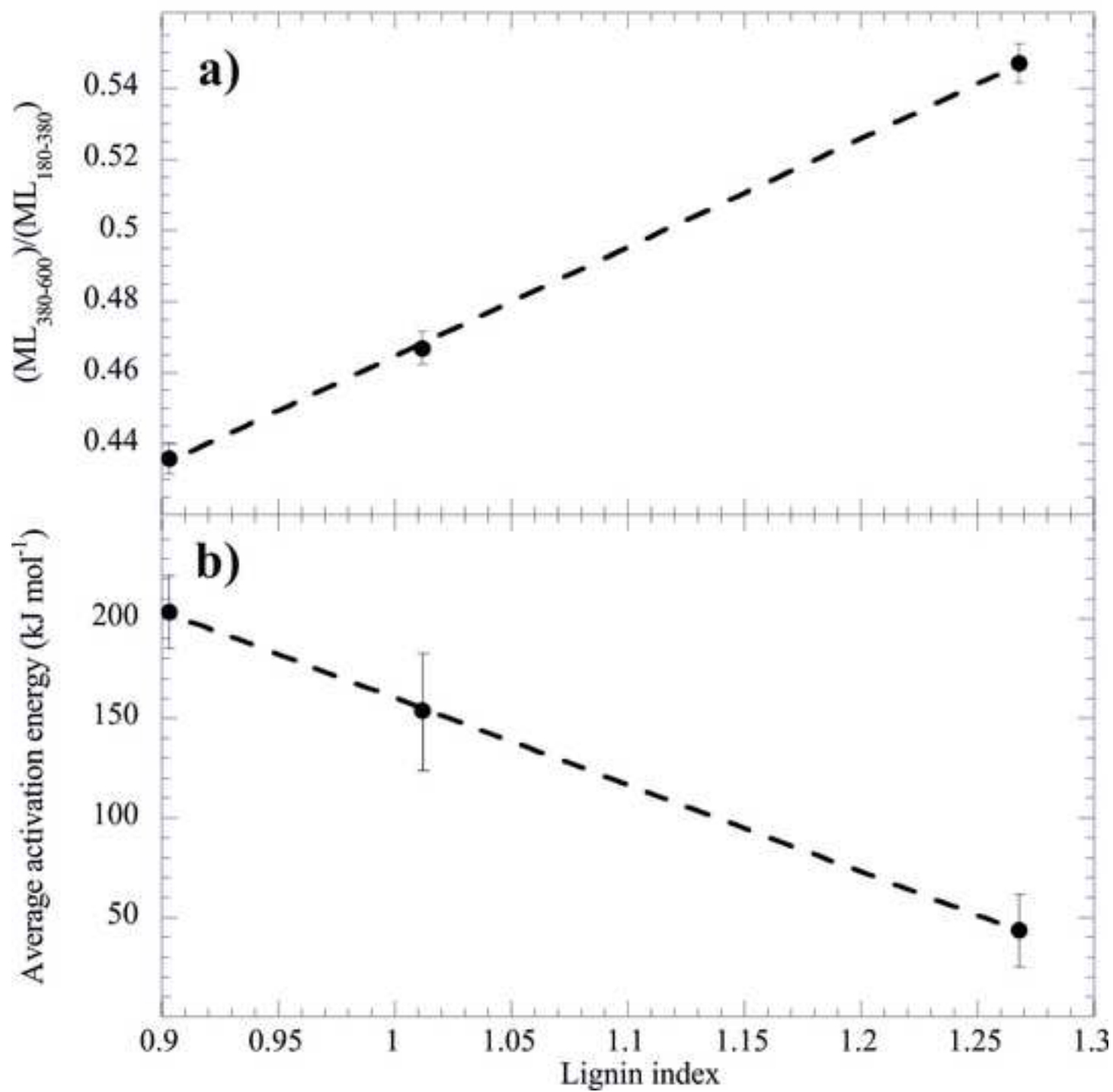


Table 1. List of the historical wooden samples

Symbol	Wood taxon	Physics apparatus	Manufacturer	Year
SM	<i>Swietenia mahagoni</i>	Chronograph tuning forks with electromagnetic drive	Max Kohl, Germany	1906
PA	<i>Picea abies</i>	Tuning forks on resonance box (sound frequency of 768 Hz)	Rudolph Koenig, France	1868
JR	<i>Juglans regia</i>	Support for tuning forks	Rudolph Koenig, France	1864

Table 2. Mass losses of the historical woods obtained by TG measurements at $\beta = 10 \text{ }^\circ\text{C min}^{-1}$

Wood	ML ₂₅₋₁₅₀ (wt%)	ML ₁₈₀₋₃₈₀ (wt%)	ML ₃₈₀₋₆₀₀ (wt%)	(ML ₁₈₀₋₃₈₀)/(ML ₃₈₀₋₆₀₀)	DTG peak ($^\circ\text{C}$)
SM	5.65 ± 0.06	64.6 ± 0.7	28.1 ± 0.3	0.435 ± 0.009	342 ± 3
PA	5.93 ± 0.06	62.0 ± 0.7	28.9 ± 0.3	0.46 ± 0.01	341 ± 3
JR	6.67 ± 0.07	57.6 ± 0.6	31.5 ± 0.3	0.54 ± 0.01	288 ± 3